

First-principles exploration of alternative gate dielectrics: Electronic structure of ZrO_2/Si and ZrSiO_4/Si interfaces

Ragesh Puthenkovilakam

Department of Chemical Engineering, University of California, Los Angeles, California 90095, USA

Emily A. Carter

Department of Chemistry and Biochemistry, University of California, Los Angeles, California 90095, USA

Jane P. Chang

Department of Chemical Engineering, University of California, Los Angeles, California 90095, USA

(Received 12 May 2003; revised manuscript received 17 October 2003; published 28 April 2004)

We employed first principles simulations using density functional theory within the local density approximation to investigate the electronic properties of the ZrO_2/Si and ZrSiO_4/Si interfaces. We considered the interfaces between the (001) surfaces of tetragonal zirconia ($t\text{-ZrO}_2$) or zircon (ZrSiO_4) and a silicon (100) substrate. We find that ZrO_2/Si interfaces exhibit partial occupation of zirconium dangling bonds (Zr d states) at the Fermi level when the zirconium coordination is reduced from its bulk coordination. Hydrogen passivation of zirconium atoms, as well as oxygen bridging at the interface, can remove the partial occupancy of d orbitals at the Fermi level. The calculated band offsets of these interfaces show asymmetric band alignments, with conduction band offsets between 0.64 and 1.02 eV and valence band offsets between 3.51 and 3.89 eV, depending on the zirconium and oxygen coordination at various ZrO_2/Si interfaces. By contrast, the ZrSiO_4/Si interface shows no partial occupation of zirconium dangling bonds at the Fermi level and provides a more symmetric band alignment, with a much higher conduction band offset of 2.10 eV and a valence band offset of 2.78 eV. These results suggest that ZrSiO_4 may form an excellent interface with silicon in terms of its electronic properties and therefore may be a suitable candidate for replacing SiO_2 as a gate insulator in silicon-based field effect transistors. On the other hand, we suggest that ZrO_2 will require additional interface preparation or postdeposition annealing to yield adequate electronic properties for gate dielectric applications.

DOI: 10.1103/PhysRevB.69.155329

PACS number(s): 73.20.At, 73.40.Qv

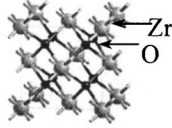
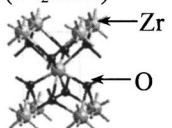
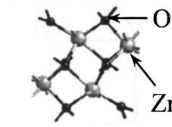
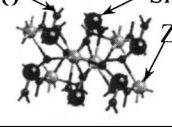
I. INTRODUCTION

The rapid scaling of silicon-based metal-oxide-semiconductor field effect transistor (MOSFET) devices has led to gate insulating films less than 5 nm thick, where quantum mechanical tunneling currents significantly reduce the insulating behavior of the gate dielectric.^{1,2} In order to overcome this problem, several alternative dielectrics have been proposed and investigated, with the goal of replacing conventional SiO_2 gate oxides. The strategy is to exploit the higher dielectric constant (k) materials so that a thicker gate insulator can be used, while maintaining the required overall gate capacitance. Among many possible candidates, transition metal oxides and silicates such as ZrO_2 , ZrSiO_4 , HfO_2 , and HfSiO_4 have attracted much attention due to their relatively large dielectric constant, high band gap, high breakdown field, and good thermal stability in contact with silicon.²⁻⁴ Material characteristics of these films deposited on silicon have been studied extensively using a variety of experimental techniques, and MOSFET devices fabricated using these films showed excellent electrical characteristics.^{2,5-9} More recently, there have been a number of first principles studies focusing on the bulk electronic properties of these thin films using density functional theory (DFT).¹⁰⁻¹⁷ However, as the thickness of the dielectric decreases, the electronic and material properties of the dielectric/Si interface will dominate the overall device performance and a thorough understanding of this interface is essential in designing better devices. In order to use ZrO_2

and ZrSiO_4 as gate dielectric materials in complimentary MOSFET's, they should have sufficiently high (> 1.00 eV) tunneling barriers to both holes and electrons.¹⁸ These barriers correspond to conduction and valence band offsets between the semiconducting silicon substrate and the insulating dielectrics, and a quantification of this offset is essential in understanding the transport properties of MOSFET devices. Although there have been a number of first principles studies analyzing the SiO_2/Si interface in detail,¹⁹⁻²⁸ very few studies have examined the detailed electronic and atomic structure of high- k dielectric/Si interfaces.^{12,29-33} For example, Fiorentini and Gulleri²⁹ evaluated the band offsets of both zirconia and hafnia films on silicon, though the electronic structures of the interfaces were not discussed in detail.

In this work we explore the detailed atomic and electronic structure of ZrO_2/Si and ZrSiO_4/Si interfaces in an attempt to understand the relation between the atomic structure at the interface and the underlying electronic properties. In the second section, details of the calculation method are presented. In the third section, bulk properties of silicon, ZrO_2 , and ZrSiO_4 are calculated and compared with experimental data and previous theoretical results whenever available. The fourth section discusses the properties of $\text{Si}(100)$, $t\text{-ZrO}_2(001)$, and $\text{ZrSiO}_4(001)$ surfaces, which are subsequently used to construct the relevant interfaces. The fifth section describes the calculations of electronic band gaps and interface states for dielectric/Si interfaces, with an emphasis

TABLE I. Structural and electronic parameters of relaxed bulk phases of Si, ZrO₂, and ZrSiO₄.

Optimized Bulk unit cells	Lattice constants (Å)		Energy (eV)/ Formula unit		E_g^a (eV)	ϵ_∞^b	
	This work	Expt. ^c	This work	Expt. ^d	This work	This work	other DFT ^e
Si (<i>Fd-3m</i>) 	$a=5.41$ $b=5.41$ $c=5.41$	$a=5.43$ $b=5.43$ $c=5.43$			0.50		
c-ZrO ₂ (<i>Fm-3m</i>) 	$a=5.03$ $b=5.03$ $c=5.03$	$a=5.09$ $b=5.09$ $c=5.09$	0.000	0.000	3.40	5.09	5.75
t-ZrO ₂ (<i>P4₂/nmc</i>) 	$a=3.59$ $b=3.59$ $c=5.18$	$a=3.57$ $b=3.57$ $c=5.18$	-0.050	-0.057	3.90	5.26	5.59
m-ZrO ₂ (<i>P2₁/c</i>) 	$a=5.11$ $b=5.28$ $c=5.26$	$a=5.15$ $b=5.21$ $c=5.32$	-0.100	-0.120	3.50	4.80	
ZrSiO ₄ (<i>I4₁/amd</i>) 	$a=6.53$ $b=6.53$ $c=5.91$	$a=6.54$ $b=6.54$ $c=5.92$			4.84	4.14	4.16

^a E_g = Band gap (eV).

^b ϵ_∞ = Static dielectric constant.

^cReferences 47, 73, and 74.

^dReference 75.

^eReferences 14 and 15.

on the effect of various zirconium or oxygen coordination at the interface. The sixth section describes the calculation of band offsets of dielectric/Si interfaces with a discussion on the effect of different atomic bonding arrangements at the interfaces on the corresponding band alignments.

II. CALCULATION DETAILS

All calculations in this work were performed using the CASTEP program,^{34,35} which employs the plane wave pseudo-potential method to calculate the total energy within the framework of the Kohn-Sham DFT.³⁶⁻³⁸ We used the local

density approximation (LDA) for the exchange-correlation functional, since electronic properties (such as band gaps) are not improved significantly using a generalized gradient approximation (GGA) to exchange and correlation.³⁹ We utilized Vanderbilt ultrasoft pseudopotentials,⁴⁰ the default pseudopotentials provided in CASTEP, which allow numerically converged calculations at relatively low kinetic energy cutoffs of the plane wave basis. The 4*s* and 4*p* semicore electrons were included explicitly for Zr, along with the valence electrons of all elements. Pseudo-wave-functions were expanded in plane waves up to a kinetic energy cutoff of 500 eV, and the Brillouin zone was sampled by a Monkhorst-

Pack mesh of k points with a k -point spacing of 0.07 \AA^{-1} . The total energy was converged to within 0.01 eV/atom under these conditions. Electronic relaxation was performed using the Pulay density mixing along with the conjugate gradient minimization method.^{38,41} Ionic relaxation was performed using Broyden-Fletcher-Goldfarb-Shanno (BFGS) update scheme,⁴² until the root-mean-square forces on the atoms were less than 0.05 eV/\AA . Symmetry constraints were imposed appropriate to the space group of the crystalline phases for bulk calculations and no symmetry constraints were imposed for surface and interface calculations.

Bulk properties of silicon, ZrO_2 , and ZrSiO_4 are well studied experimentally^{8,43} and theoretically.^{14–17,44} For silicon, we examined the most relevant crystal structure for microelectronics applications, a diamond lattice with a space group of $Fd\bar{3}m$. ZrO_2 undergoes polymorphic transformations as the temperature changes; the relevant crystal structures are given in Table I. At high temperatures ($T > 2350 \text{ }^\circ\text{C}$), it adopts a cubic structure ($Fm\bar{3}m$), while at low temperatures ($T < 1150 \text{ }^\circ\text{C}$) a monoclinic ($P2_1/c$) structure is preferred.⁴⁵ A tetragonal phase exists at intermediate temperatures; it can be viewed as a simple perturbation of the cubic phase, in which the oxygen atoms are displaced alternately along the 4_2 axis, resulting in a $P4_2/nmc$ symmetry.⁴⁶ In cubic and tetragonal ZrO_2 , Zr is eightfold coordinated and O is fourfold coordinated; in the monoclinic structure, Zr is sevenfold coordinated while the oxygen atoms are triply and quadruply bonded. ZrSiO_4 is primarily known as zircon, with a space group of $I41/amd$, with eightfold coordinated Zr and threefold coordinated O (Table I). Crystal structures were optimized for silicon and three phases of ZrO_2 and ZrSiO_4 , and the relaxed geometries were used to calculate their electronic band structures.

Before forming interfaces, it is important to understand the surface structures that dictate the interface formation. For calculating the surface electronic structures of silicon, ZrO_2 , and ZrSiO_4 , we used a repeated slab geometry with a vacuum thickness of 12 \AA in the c direction to avoid spurious interactions between periodic images of the slabs. The Si(100) surface is considered in this work because it is the most favored surface in MOSFET devices due to its low interface state density and correspondingly superior electrical characteristics. The Si(100) surface was simulated using a slab calculation consisting of seven layers of Si, which is sufficient for convergence of surface energies,⁴⁷ as shown in Fig. 1(a). The bottom silicon layer was passivated with hydrogen to facilitate the convergence of the self-consistent calculation. Unit cell dimensions were kept fixed at $a = 7.65 \text{ \AA}$, $b = 3.83 \text{ \AA}$ (corresponding to the fully relaxed bulk unit cell), as were the atoms in the bottom four layers, while all the other atoms were allowed to relax. We selected $t\text{-ZrO}_2$ for the surface and interface calculations because it has been shown to exist even at low temperatures,⁴⁸ and sometimes coexists with the monoclinic phase on silicon.⁹ The (001) surface of the tetragonal phase is selected, because it forms a lattice-matched interface with Si(100) with a minimum number of dangling bonds. We chose a slab consisting of 4 layers of ZrO_2 and 12 \AA of vacuum, such that the surfaces on each side of the slab are essentially equivalent, as

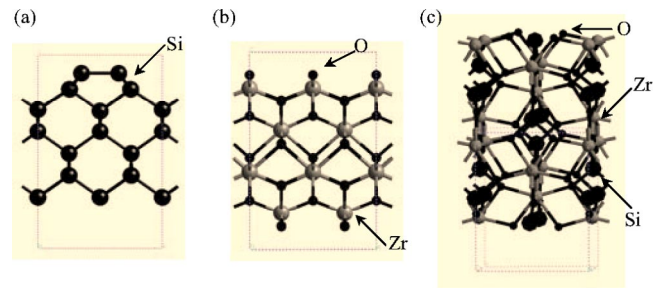


FIG. 1. The relaxed unit cells of (a) Si(100)- 2×1 , (b) $t\text{-ZrO}_2(001)$, and (c) $\text{ZrSiO}_4(001)$ surfaces.

shown in Fig. 1(b). In this structure, the surface coordination numbers of Zr and O becomes six and two, respectively, compared to their bulk coordination numbers of eight and four. Slab unit cell dimensions were kept fixed at $a = 7.19 \text{ \AA}$, $b = 3.59 \text{ \AA}$ (corresponding to the fully relaxed bulk unit cell) and all the atoms were allowed to relax. A layering sequence of $|\text{O}-\text{Zr}-\text{O}|\text{O}-\text{Zr}-\text{O}|..$ is adopted to form a stoichiometric slab of ZrO_2 , following the procedure outlined by Christensen and Carter.⁴⁹ This layer association makes the surface nonpolar and stoichiometric. For ZrSiO_4 , the (001) surface was chosen because $\text{ZrSiO}_4(001)/\text{Si}(100)$ interface geometry reproduced the Si $2p$ core level shifts observed in thin films of ZrSiO_4 on silicon (100) surface.³⁰ We chose a stoichiometric slab of 8 layers of ZrSiO_4 for the calculation, as shown in Fig. 1(c). At the surface, the Zr coordination reduces to six from its bulk coordination of eight, while the Si coordination reduces to two from its bulk coordination of four. Note that O coordination remains at three. The dangling bonds of silicon at the bottom surface were passivated with H to allow convergence in the calculation. Specific calculation details of the surface calculations are summarized in Table II.

For the dielectric/Si interface calculations, we used a repeated slab geometry with 12 \AA of vacuum between the slabs. All the atoms in the bottom silicon layer were passivated with hydrogen to allow convergence in the self-consistent calculations. For the geometry optimization, the unit cell dimensions (Table III) and all the Si atoms in the bottom 4 layers were kept fixed, while all other atoms in the

TABLE II. Computational details for surface calculations (vacuum thickness, 12 \AA ; k -point spacing, 0.07 \AA^{-1}).

Surfaces	Unit cell size (\AA)	No. of layers	Surface energy
Si(100)	$a = 7.65$ $b = 3.83$ $c = 22.0$	7	NA ^a
$t\text{-ZrO}_2(001)$	$a = 7.19$ $b = 3.59$ $c = 22.0$	4	1.980 J/m ²
$\text{ZrSiO}_4(001)$	$a = 6.54$ $b = 6.54$ $c = 23.0$	8	NA

^aNA denotes not available.

TABLE III. Computational details for interface calculations (vacuum thickness, 12 Å; k -point spacing, 0.07 \AA^{-1}).

Interfaces	Unit cell size ^c (Å)	No. of layers ^d	No. of layers ^e
$t\text{-ZrO}_2(001)/\text{Si}(100)\text{-}2 \times 1$	$a=7.65$ $b=3.83$ $c=32.0$	3, 7	5, 7
$t\text{-ZrO}_2(001)/\text{Si}(100)\text{-}2 \times 1^a$	$a=7.65$ $b=3.83$ $c=32.0$	3, 7	5, 7
$t\text{-ZrO}_2(001)/\text{Si}(100)^b$	$a=3.83$ $b=3.83$ $c=32.0$	3, 7	5, 7
$\text{ZrSiO}_4(001)/\text{Si}(100)$	$a=5.41$ $b=5.41$ $c=32.0$	4, 7	8, 7

^aHydrogen-passivated Zr at interface to make Zr eightfold coordinated.

^bBridging oxygen at interface with unreconstructed Si(100).

^cCorresponds to optimized bulk unit cell dimension of Si.

^dFor electronic band structure calculations.

^eFor band offset calculations.

unit cell were allowed to relax to partially relieve the interfacial strain. We found that the first three silicon layers close to the interface have to be relaxed in order for the forces in the adjacent fixed layer (i.e., the fourth silicon layer from the interface) to be less than 0.05 eV/\AA . To form the $\text{ZrO}_2(001)/\text{Si}(100)$ interface, since the calculated bulk lattice constants of silicon and $t\text{-ZrO}_2$ are 5.41 \AA and 5.08 \AA ($\sqrt{2} \times 3.59 \text{ \AA}$), respectively, the ZrO_2 unit cell was expanded from 5.08 \AA to 5.41 \AA to form a coherent interface. Because of the atomic density difference between $t\text{-ZrO}_2$ and silicon, there are more dangling bonds at the $t\text{-ZrO}_2(001)$ surface than at a reconstructed silicon surface. Due to this mismatched number of dangling bonds, Zr and O at the interface become six- and threefold coordinated, respectively, different from their eight- and fourfold bulk coordinations, as shown in Fig. 2(a), where the slabs used in the $t\text{-ZrO}_2/(001)/\text{Si}(100)$ interface calculations consisted of 7 layers of silicon, 3 layers of ZrO_2 . The 3 layers of ZrO_2 were chosen to be stoichiometric and nonpolar, to avoid artificial charge transfer from one surface to another.⁴⁷ Two additional $t\text{-ZrO}_2(001)/\text{Si}(100)$ interfaces were considered with different atomic bonding arrangements. In one case, the Zr atoms at the interface were passivated by hydrogen so that they retain their bulk coordination of eight. In the other case, oxygen coordination at the interface was reduced from 3 to 2. This was achieved by removing the twofold coordinated oxygen atoms from the $t\text{-ZrO}_2(001)$ surface and bridging the Zr atoms to the unreconstructed Si(100) surface by means of twofold coordinated oxygen atoms. To form the $\text{ZrSiO}_4(001)/\text{Si}(100)$ interface, we compressed the bulk ZrSiO_4 structure along the [100] and [010] directions by the ratio of the lattice constants of silicon and ZrSiO_4 and expanded it in the [001] direction to restore the bulk ZrSiO_4 density and attached it to the Si(100) surface only through bridging oxygen atoms,³⁰ as shown in the relaxed structure in Fig. 2(b). Since the lattice mismatch of this interface is

high, we performed our calculations with a larger unit cell size ($a=b=10.82 \text{ \AA}$) and found no appreciable change in the structural parameters. The slab used in the calculation consisted of 7 layers of Si and 4 layers of ZrSiO_4 . Once the interfaces are relaxed, the resulting geometries were used to calculate single point energies and band structures. Densities of states (DOS) were calculated using a Gaussian smearing scheme as implemented in CASTEP using a smearing width of 0.2 eV . Partial densities of states (PDOS) were calculated by projecting the plane wave states onto a localized atomic basis set.⁵⁰ Localized atomic orbitals were generated by solving for the lowest energy eigenstates of the pseudopotential in a sphere (cutoff radius of 15 a.u.), using a spherical Bessel function basis set, as implemented in CASTEP.^{51,52} The coordination numbers are determined based on a radial cutoff of 3 \AA . Energy levels for the band structure and DOS and PDOS plots are referenced to the valence band maximum, which is set to 0.00 eV . The elec-

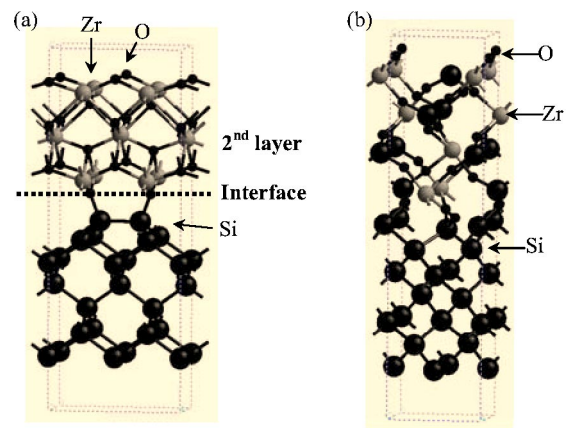


FIG. 2. The relaxed unit cells of (a) $t\text{-ZrO}_2(001)/\text{Si}(100)2 \times 1$ and (b) $\text{ZrSiO}_4(001)/\text{Si}(100)$ interfaces.

tronic contribution of the static dielectric constant (ϵ_∞) is calculated using Fermi's golden rule approximation as implemented in CASTEP. Since the LDA band gaps are underestimated, we used a scissor operator⁵³ to shift the conduction bands rigidly to match the experimental band gaps (5.65 eV for ZrO_2 and 6.00 eV for ZrSiO_4),^{54,55} and the resulting eigenvalues are used to calculate the transition matrix elements for the calculation of static dielectric constant.

For calculating the electrostatic potential distributions required for band offset calculations, we used 5 layers of ZrO_2 and 8 layers of ZrSiO_4 (Table III) for their respective interfaces with silicon, since the electrostatic potential distribution converges much slower than the total energy and the density of states.

III. BULK CALCULATIONS

In the current work, the lattice constant of bulk silicon is calculated to be 5.41 Å, very close to the experimental lattice constant of 5.43 Å. Though the calculated LDA band gap (~ 0.50 eV) of silicon is only $\sim 50\%$ of the experimental band gap (1.12 eV),⁴⁷ other structural parameters (bulk modulus, elastic constants) and the electronic band structure are well described by DFT-LDA.⁴⁷ Due to the intrinsic errors of the LDA, we only use the band gaps to assess qualitative trends.

The calculated optimized lattice constants of the three phases of ZrO_2 are compared with previously reported experimental results, showing excellent agreement (Table I). The relative energies of the three phases have the correct phase ordering, with the monoclinic phase lowest in energy, and are in excellent agreement with previously reported values using the full potential linear augmented plane wave method (FLAPW).^{14,17,56} The electronic contribution of the static dielectric constant calculated using Fermi's golden rule approximation for all three phases, was approximately the same, 4.80–5.26, and accounts for less than 30% of the measured dielectric constants of ZrO_2 that range from 18 to 31.^{14,29} This suggests that the predominant contribution to the dielectric constant stems from the ion-ion interaction in these ionic crystals.

The electronic band structure, density of states (DOS), and the projected density of states (PDOS) of tetragonal ZrO_2 are shown in Figs. 3(a) and 3(b). An indirect LDA band gap of 3.90 eV is observed, smaller than the measured band gap of ZrO_2 , 5.65 eV.⁵⁴ This disparity in the band gap is expected, since it is well known that LDA underestimates the band gaps of insulators. The valence band is primarily formed by O p states while the conduction band is derived from Zr d states. The Zr s and p states remain largely core-level-like. The observed nonempty Zr valence band results from incomplete charge transfer between Zr and O, and is consistent with the previously reported results on ZrO_2 .^{44,49} This partial covalent bonding has implications for the electronic properties, as discussed below. The calculated band structures of cubic and monoclinic phases showed LDA band gaps of 3.40 eV and 3.50 eV, respectively, also in excellent agreement with earlier LDA results.^{17,57} The corresponding PDOS of the cubic phase showed a valence band-

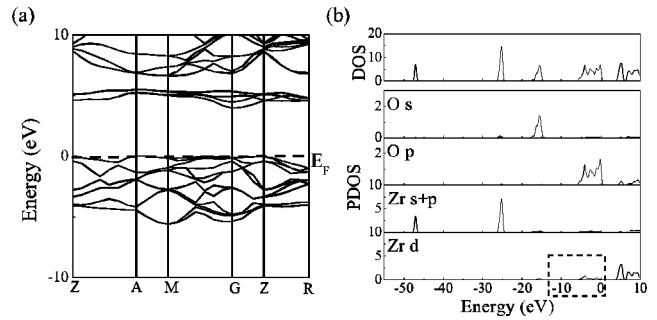


FIG. 3. Bulk t - ZrO_2 : (a) The electronic band structure and (b) the total and projected density of states. Note that the Zr d valence band is partially occupied, as circled by the dotted line in (b), indicating a partial Zr—O covalent interaction.

width similar to that of the tetragonal phase (6.5 eV and 6.7 eV, respectively), while the monoclinic phase showed a decrease in the valence bandwidth (5.7 eV) due to its reduced average O coordination.

Table I provides an optimized geometry of ZrSiO_4 , where we find a Si—O bond length of 1.62 Å and Zr—O bond lengths of 2.09 Å and 2.25 Å, corresponding to two different bridging Zr—O—Si bonds. The electronic structure [Fig. 4(a)] yields an LDA band gap of 4.84 eV, which is $\sim 80\%$ of the experimentally observed band gap (6.00 eV).⁵⁵ As in ZrO_2 , Zr d states form the lower conduction band while O p states form the upper valence band [Fig. 4(b)]. The Zr—O bond is predominantly ionic where Zr transfers most of its valence electrons to O, with only a very small covalent component from the interaction of Zr d and O p states, as indicated by the small amplitude of the PDOS within the dotted rectangle in Fig. 4(b). The Si—O bond is partially covalent due to interactions of Si p and O p states [between -10 eV and 0 eV in Fig. 4(b)].

IV. SURFACE CALCULATIONS

The symmetric dimer configuration of the Si(100) surface, as shown in Fig. 1(a), exhibits metallic character. We note that the symmetric dimer configuration is more relevant in constructing the interfaces, because at the typical deposition temperatures of ZrO_2 , asymmetric buckling is effectively

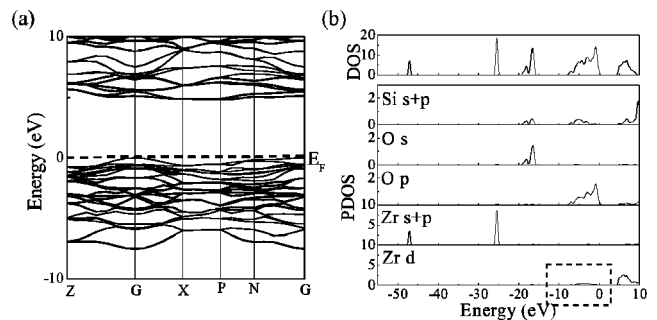


FIG. 4. Bulk ZrSiO_4 : (a) The electronic band structure and (b) the total and projected density of states. Note that Zr d valence band is nearly empty, as circled by the dotted line in (b), indicating only a small covalent component to the Zr—O bonding.

destroyed by thermal fluctuations.^{58,59} Moreover, during interface formation, whether the Si(100) surface remains reconstructed depends on the detailed reaction mechanisms involved in the deposition of metal oxides on silicon. In fact, simulations of the reaction mechanism of crystalline silicon deposition from silane precursors show that the dimers at the silicon surface open up during the initial stage of the deposition.⁶⁰ To account for both possibilities, we consider both unreconstructed and reconstructed Si(100) surfaces in our interface models. To concisely discuss our findings, unless specified, results included are from reconstructed Si(100)-2×1 surfaces. The optimized Si(100) surface yields a dimer bond length of 2.20 Å and a Si-Si back bond length of 2.25 Å, in excellent agreement with previously reported values.^{47,61} The electronic band structure showed partial occupation of Si dangling bond states (contrary to bulk silicon), as evidenced in Figs. 5(a) and 5(b), consistent with previously reported results that the symmetric dimer configuration of Si(100)-2×1 surface gives rise to partially occupied dangling bond states.^{62,63}

For the *t*-ZrO₂(001) surface, the optimized structure did not result in any surface reconstruction. The calculated relaxed and unrelaxed surface energies of *t*-ZrO₂(001) (1.503 J/m² and 1.980 J/m²) agree well with LDA values reported by Christensen and Carter (1.577 J/m² and 1.961 J/m²).^{44,49} We calculated an LDA band gap for the *t*-ZrO₂(001) surface of 2.50 eV, much less than the LDA band gap of bulk *t*-ZrO₂ (3.90 eV). This is due to the reduction of the Zr and O surface coordination to six and two, respectively, compared to their bulk coordination numbers of eight and four, which introduces states [Zr *d* and O *p*, shown in dotted rectangles in Fig. 5(c)] that lie in the fundamental band gap of ZrO₂.

For the ZrSiO₄(001) surface, no surface reconstruction was observed upon relaxing the geometry. The PDOS exhibits partial occupation of states at the Fermi level, as shown in

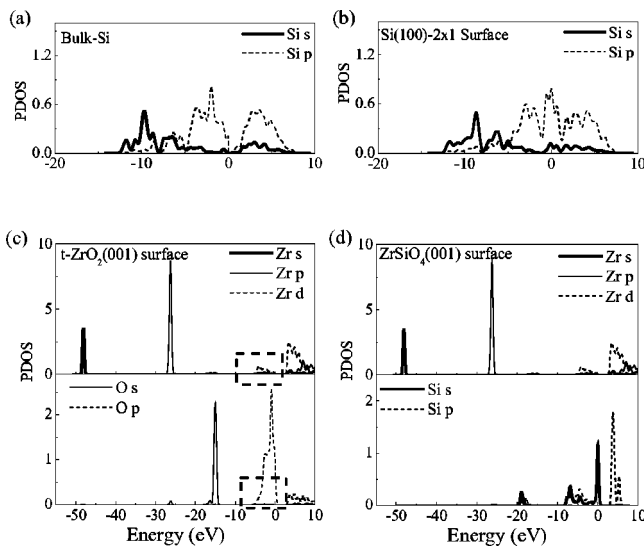


FIG. 5. The projected density of states of Si (a) in the bulk and (b) at a Si(100)-2×1 surface, (c) the projected density of states of Zr and O at a *t*-ZrO₂(001) surface, and (d) the projected density of states of Zr and Si at a ZrSiO₄(001) surface.

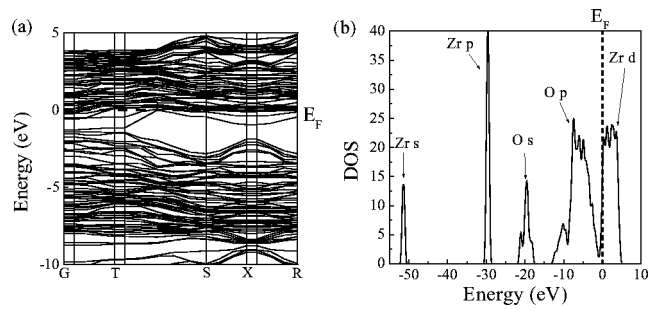


FIG. 6. The *t*-ZrO₂(001)/Si(100)-2×1 interface: (a) the electronic band structure and (b) the total density of states. The Fermi level is referenced to 0.00 eV and Zr is six-fold coordinated at the interface.

Fig. 5(d). These states can be attributed to the dangling bond states of Si at the ZrSiO₄(001) surface as evident from a sharp peak at 0.00 eV of the Si *s* and *p* states. This partial occupation is similar to what is observed for the symmetric dimer configuration of the Si(100) surface.

V. INTERFACE CALCULATIONS

A. The *t*-ZrO₂(001)/Si(100) interfaces

The optimized *t*-ZrO₂(001)/Si(100)-2×1 geometry yields Zr—O bond lengths of 1.97 Å at the interface and 2.10–2.30 Å in all other layers. The reduced Zr—O bond length at the interface corroborates the intrinsic strain at the interface due to the lattice mismatch. The Si—O bond length at the interface was found to be 1.67 Å, very close to the measured Si—O bond length of crystalline SiO₂.⁶⁴

The optimized structure of the *t*-ZrO₂(001)/Si(100)-2×1 interface was used to calculate the electronic band structure. We find no band gap, as shown in Fig. 6(a). To properly interpret the calculated band gaps in this work, it is important to note that the calculated LDA band gap of a SiO₂/Si interface is 1.30 eV.²⁰ The corresponding DOS spectrum of *t*-ZrO₂(001)/Si(100)-2×1 interface clearly shows that Zr *d* states are partially occupied at the Fermi level [Fig. 6(b)]. To assess the effect of interface formation, the projected Zr and O densities of states of the interface are shown in Figs. 7(a) and 7(b). The Zr states starting at the second layer resemble

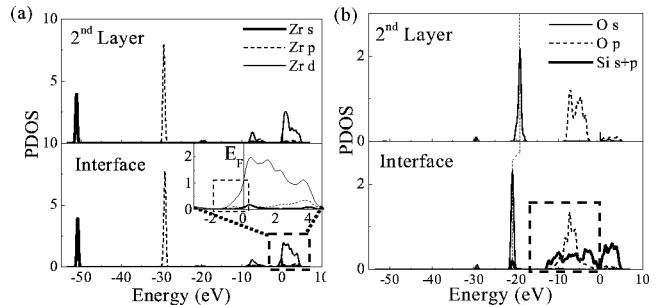


FIG. 7. The *t*-ZrO₂(001)/Si(100)-2×1 interface: The projected density of states of (a) Zr and (b) O at the interface and the next nearest layer to the interface. The inset of (a) shows the Zr *d* levels, which are partially occupied at the Fermi level.

TABLE IV. Effect of Zr and O coordinations on the interface electronic structure.

Interface	Zr coord. at interface	O coord. at interface	LDA band gap of interface (eV)
β -cristobalite $\text{SiO}_2/\text{Si}(100)^a$	4	2	1.30
$t\text{-ZrO}_2(001)/\text{Si}(100)\text{-}2\times 1$	6	3	~ 0.00
$t\text{-ZrO}_2(001)/\text{Si}(100)\text{-}2\times 1^b$	8	3	0.50
$t\text{-ZrO}_2(001)/\text{Si}(100)^c$	6	2	0.10
$t\text{-ZrO}_2(001)/\text{Si}(100)^d$	6	4	0.00
$t\text{-ZrO}_2(001)/\text{Si}(100)^e$	8	4, 2	0.60
$\text{ZrSiO}_4(001)/\text{Si}(100)$	4	2	1.00

^aReference 20.

^bHydrogen-passivated Zr at interface to make Zr eightfold coordinated.

^cBridging oxygen at interface with unreconstructed $\text{Si}(100)$.

^dUnreconstructed $\text{Si}(100)$.

^eUnreconstructed $\text{Si}(100)$ with excess oxygen at the interface to make Zr eightfold coordinated.

those observed in bulk ZrO_2 , where no partial occupation of Zr d states at the Fermi level was observed. The Zr $4s$ and $4p$ semicore levels state at -48.00 eV and -27.00 eV, respectively, are sharply peaked, indicating their nonbonding nature. The width of the O p valence band is 9.50 eV at the interface [see dotted rectangle in Fig. 7(b)], compared to bandwidths of 5.65 eV in the second and other layers. This broadening of the O p valence band is a direct result of the hybridization of O and Si states at the interface, causing an upward shift of the valence band maximum. This intermixing of silicon and oxygen states is characteristic of Si—O covalent bonding.

To understand the detailed electronic occupation of the interface atoms, it is necessary to consider carefully the bonding arrangement at the interface. When a $t\text{-ZrO}_2(001)$ surface is brought in close contact to a $\text{Si}(100)\text{-}2\times 1$ surface, Si—O bond formation at the interface increases the O coordination from two to three. Though silicon is more electronegative than zirconium, this Si—O bonding reduces the charge transfer from zirconium to oxygen compared to what was observed in bulk ZrO_2 . This is evident from the PDOS spectrum where the interface Zr d states show increased occupation [inset in Fig. 7(a)]. It is important to note that this partial occupation of Zr d states at the Fermi level is confined to the first ZrO_2 layer [i.e., the interfacial layer; see Fig. 7(a)], which is equivalent to about 3.50 \AA of ZrO_2 . Starting from the second layer, the Zr PDOS is identical to what is found for bulk $t\text{-ZrO}_2$. Since these partially occupied states are localized close to the ZrO_2/Si interface, they fall under the general category of virtual gap states (VGS's) and their significance with respect to the alignments of bulk bands will be discussed in detail in the sixth section.

Since the VGS's result from the coordination change of zirconium and oxygen, it is important to understand the effect of interface coordination numbers on the resulting electronic structure. It is indeed possible to create a zirconium coordination of eight at the interface by having a higher oxygen concentration at the interface (Table IV, row 6). Realistically, this is not likely, since bulk ZrO_2 is well known for its oxygen deficiency. Instead, we investigate the effect of

hydrogen passivation of the interface, where the Zr coordination becomes eightfold. This approach has allowed the investigation of the effect of coordination at the SiO_2/Si interface, and can be tested experimentally via postdeposition annealing in H_2 .^{65,66} The electronic structure of this interface is shown in Figs. 8(a) and 8(b), and a direct LDA band gap of 0.50 eV is observed for this interface. The projected density of states of Zr indicates that the Zr d levels form a small set of bands below the valence band maximum of the interface, and hence are fully occupied [insets in Fig. 8(c)]. Since the O s and p states for this interface [Fig. 8(d)] show the same characteristics as that of the interface without hydrogen

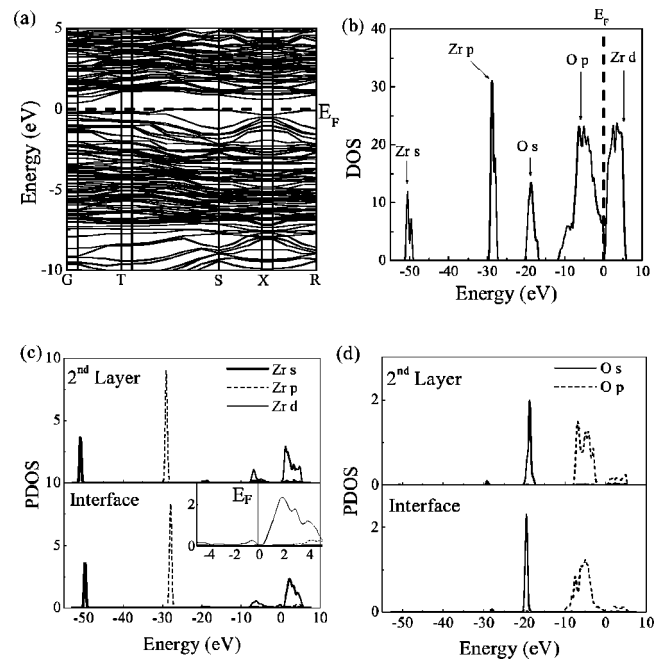


FIG. 8. The $t\text{-ZrO}_2(001)/\text{Si}(100)\text{-}2\times 1$ interface with H passivation: (a) the electronic band structure, (b) the total density of states, (c) the projected density of states of Zr, and (d) the projected density of states of O. The interface shows an insulating character.

passivation, it is evident that attachment of hydrogen atoms to Zr splits the partially occupied Zr d levels, removing the degeneracy and hence the partial occupation. The position of these energy levels with respect to the bulk bands will also be discussed later in the sixth section.

In addition to the reduced Zr coordination that makes the Zr $4d$ levels partially occupied, O coordination could also affect the electronic structure. To investigate this effect, we considered a t -ZrO₂(001)/Si(100) interface in which the t -ZrO₂(001) surface is attached to the Si(100) surface through bridging oxygen atoms. In this case, the surface Zr coordination is six while the O coordination is reduced from three to two. Since the O is only twofold coordinated, electrons from Zr $4d$ levels are more easily transferred to O p levels, leaving the Zr $4d$ levels unoccupied and yielding an LDA band gap of 0.10 eV. These results are summarized in Table IV, which clearly shows that the local bonding arrangement at the interface, particularly the metal-oxygen-silicon bonds, can have a significant impact on the resulting electronic characteristics of the interface.

B. The ZrSiO₄(001)/Si(100) interface

For the ZrSiO₄(001)/Si(100) interface, due to the larger intrinsic lattice mismatch (>10%) compared to the t -ZrO₂/Si interface, the Si—O bond lengths changed from their bulk value of 1.62 Å to 1.58 Å at the interface and to 1.65 Å starting from the second layer, while the Zr—O bond lengths decreased to 1.95–2.10 Å for the optimized geometry. The most important effect of the interfacial lattice mismatch is that the effective coordination of Zr atoms was reduced to four from their surface coordination of six while the O coordination was reduced from three to two. This reduced effective coordination affects the entire ZrSiO₄ layer, i.e., the coordination of all Zr atoms were changed to be the same (four). This is different from the t -ZrO₂(001)/Si(100) interface where the Zr atoms at the interface have different coordination from those away from the interface. The resulting band structure is shown in Fig. 9(a). The calculated LDA band gap of this interface is ~ 1.00 eV, much larger compared to that of a t -ZrO₂(001)/Si(100) interface and very comparable to that of a SiO₂/Si interface (1.30 eV).²⁰ This indicates that the ZrSiO₄(001)/Si(100) interface has fewer interface states compared to the t -ZrO₂(001)/Si(100)

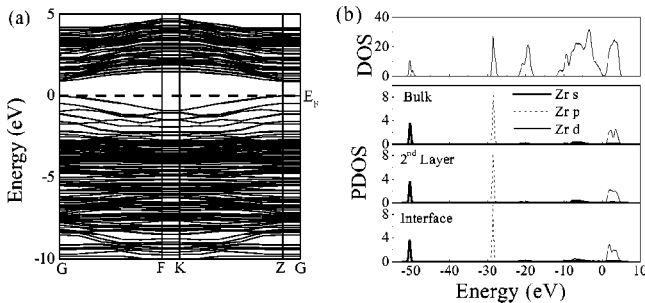


FIG. 9. The ZrSiO₄(001)/Si(100) interface: (a) the electronic band structure, (b) the total density of states and the projected density of states of Zr. There is no partial occupation of Zr d states at the Fermi level.

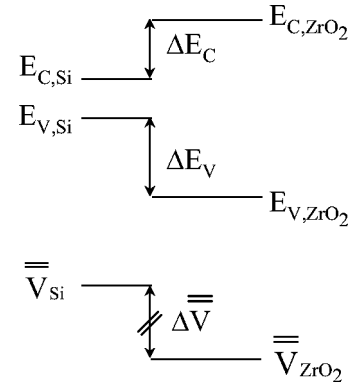


FIG. 10. The band alignment method proposed by van de Walle and Martin for heterojunctions (Ref. 67). E_C , E_V , and \bar{V} denote the conduction band minimum, valence band maximum, and the macroscopically averaged electrostatic potential.

interface. The projected density of states of Zr atoms also shows clearly that the Zr d levels are unoccupied [Fig. 9(b)], thus the corresponding band alignment with silicon is also different from that of ZrO₂, as we discuss in the next section.

VI. BAND OFFSETS

To properly compare the band energies of ZrO₂ and ZrSiO₄ to silicon, we adopt a method proposed by van de Walle and Martin,⁶⁷ in which the individual band energies in each material are referenced to the macroscopically averaged electrostatic potential, $\bar{V}(z)$, in the solid. We used supercell structures both with and without vacuum (the latter constructed to have two identical interfaces in the unit cell) for the band offset calculations and obtained essentially the same valence band offset, within 0.05 eV. The method is schematically shown in Fig. 10. The electrostatic potential, including only the local part of the Kohn-Sham potential that includes ionic, Hartree, and exchange and correlation contributions, is obtained from an interface calculation, is plane-averaged in a direction parallel to the interface, and is plotted in a direction perpendicular to the interface, as shown in Fig. 11(a) for the t -ZrO₂(001)/Si(100)- 2×1 interface. The mac-

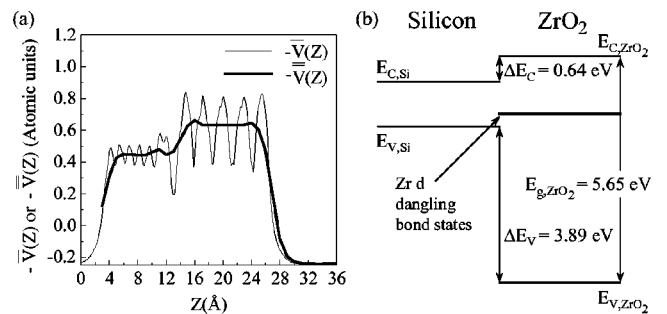


FIG. 11. The t -ZrO₂(001)/Si(100)- 2×1 interface: (a) the plane-averaged electrostatic potential and (b) the band alignment. The thick solid line represents the position of partially occupied Zr d levels. \bar{V} and \bar{V} represent the microscopically and macroscopically averaged electrostatic potentials, respectively.

TABLE V. Band offsets of various dielectric/Si interfaces.

Insulator	Interface	Zr(Si) coord. at interface	O coord. at interface	VB ^c offset (eV)	Expt. ^d E_g (eV)	CB ^e offset (eV)
ZrO ₂	<i>t</i> -ZrO ₂ (001)/Si(100)-2×1	6	3	3.89	5.65	0.64
ZrO ₂	<i>t</i> -ZrO ₂ (001)/Si(100)-2×1 ^a	8	3	3.51	5.65	1.02
ZrO ₂	<i>t</i> -ZrO ₂ (001)/Si(100) ^b	6	2	3.62	5.65	0.91
ZrSiO ₄	ZrSiO ₄ (001)/Si(100)	4	2	2.78	6.00	2.10

^aHydrogen-passivated Zr at interface to make Zr eightfold coordinated.

^bBridging oxygen at interface with unreconstructed Si(100).

^cVB denotes valence band.

^dReferences 54 and 55.

^eCB denotes conduction band.

roscopic average potential, $\bar{V}(z)$, is defined as

$$\bar{V}(z) = \frac{1}{L_1 L_2} \int_{z-L_1/2}^{z+L_1/2} \int_{z'-L_2/2}^{z'+L_2/2} \bar{V}(z'') dz'' dz',$$

where $\bar{V}(z'')$ is the microscopic average potential obtained by plane averaging the electrostatic potential, and L_1 and L_2 are lengths of a single period of the microscopic average on each side of the interface. The macroscopic average potentials away from the interface correspond to the macroscopically averaged bulk potentials of Si and ZrO₂. Thus the potential shift $\Delta\bar{V} = \bar{V}_{\text{Si}} - \bar{V}_{\text{ZrO}_2}$ can be utilized to line up the bulk energy levels of ZrO₂ and silicon, allowing the determination of the valence and conduction band offsets:

$$\Delta E_V = (E_V^{\text{Si}} - \bar{V}_{\text{bulk}}^{\text{Si}}) - (E_V^{\text{ZrO}_2} - \bar{V}_{\text{bulk}}^{\text{ZrO}_2}) + \Delta\bar{V} = 3.89 \text{ eV},$$

$$\Delta E_C = E_g^{\text{ZrO}_2} - E_g^{\text{Si}} - \Delta E_V.$$

Since LDA underestimates the band gap, we use the experimental band gaps of 1.12 eV for silicon,⁴⁷ 5.65 eV for ZrO₂,⁵⁴ and 6.00 eV for ZrSiO₄ (Ref. 55) to calculate the conduction band offsets. We calculated the conduction band offset of the *t*-ZrO₂(001)/Si(100) interface to be 0.64 eV. Moreover, the partially occupied Zr *d* bands from the inter-

face are 4.21 eV above the ZrO₂ valence band, as shown schematically in Fig. 11(b). These partially occupied states lie within the silicon band gap, forming conductive paths under an applied potential field, and thus are detrimental to the device performance. Similar calculations were performed for other ZrO₂/Si interfaces with different Zr and O coordinations; the results are given in Table V and their band alignments are shown in Figs. 12(a) and 12(b). All the valence band offsets are between 3.51 and 3.89 eV, while all the conduction band offsets are slightly less than or close to 1.00 eV. The largest conduction band offset is 1.02 eV, from the *t*-ZrO₂(001)/Si(100)2×1 interface with H-passivated Zr at the interface. The valence band offset of a ZrSiO₄(001)/Si(100) interface is 2.78 eV, resulting in a conduction band offset of 2.10 eV, giving rise to a more symmetric band alignment as shown in Fig. 13. These calculated conduction band offsets agree well with recently reported values by Fiorentini and Gulleri using the GW correction to generalized gradient approximation (GGA) eigenvalues,²⁹ but are smaller than those reported by Robertson,⁵⁵ where a model using empirical tight binding calculations and charge neutrality level (CNL) was employed.^{68,69}

These results in Table V suggest that the band alignments at the *t*-ZrO₂/Si(100) interfaces are affected by the local bonding arrangement at the interface and can be explained

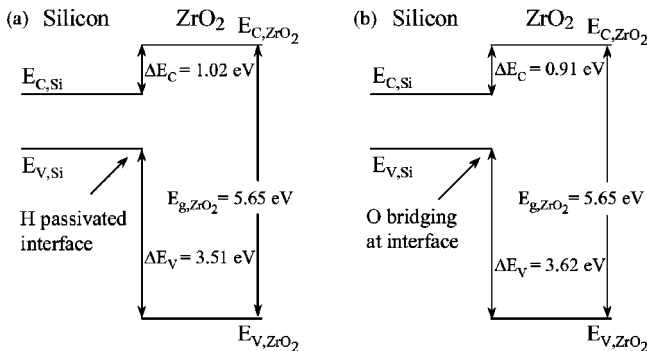


FIG. 12. Band alignment at (a) a *t*-ZrO₂(001)/Si(100)-2×1 interface with H-passivated Zr and (b) a *t*-ZrO₂(001)/Si(100) interface with bridging oxygen at the interface.

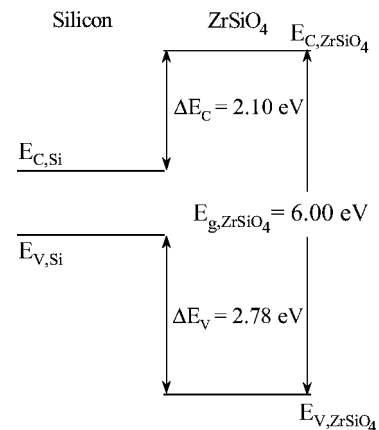


FIG. 13. The band alignment at a ZrSiO₄(001)/Si(100) interface. There are no Zr *d* states in the gap.

by the charge transfer across the interface that produces an interface dipole.^{70–72} This interface dipole forms a part of the average electrostatic potential difference ($\Delta\bar{V}$) shown in Fig. 11(a). Comparing SiO₂/Si and ZrO₂/Si interfaces, the magnitude of charge transfer depends on the difference in ionicity of zirconium and silicon. In principle, the higher the interface dipole due to charge transfer across the interface, the less the valence band offset and the higher the conduction band offset, as indicated in Fig. 10. In a Zr—O—Si bonding arrangement, charge transfer from silicon to oxygen is reduced by the presence of zirconium, which is more electropositive than silicon. Thus, a more asymmetric band alignment is expected in a ZrO₂/Si interface compared to SiO₂/Si interface. To adjust the band alignment, hydrogen passivation of the zirconium atoms at the interface is shown to allow more charge transfer from silicon to oxygen, yielding a more symmetric band alignment and hence higher conduction band offset. Therefore it is critical to maintain bulk-like Zr coordination at the interface to ensure a more symmetric band alignment and to avoid the partial occupancy of Zr *d* states at the Fermi level. In addition, bridging oxygen atoms enhance the charge transfer through Si—O bonds, giving rise to a higher conduction band offset. It is clear that altering the interface dipole in a controlled manner is an effective way of changing the band offsets at these interfaces.

The band offset of a ZrSiO₄/Si interface is quite different from that of a ZrO₂/Si interface, in that half the bonding at the ZrSiO₄/Si interface is Si—O—Si while the other half is Zr—O—Si. Thus the properties of the ZrSiO₄/Si interface are expected to be in between that of ZrO₂/Si and SiO₂/Si interfaces. This is evident from the more symmetric band alignment obtained for ZrSiO₄/Si interfaces, as shown in Fig. 13. Most importantly, the Zr coordination of a ZrSiO₄/Si interface remains at four throughout the film, eliminating the possibility of any partially occupied states at the Fermi level. These results suggest that ZrSiO₄ provides

adequate barriers for both holes and electrons conduction, making it suitable as an alternative gate dielectric in MOSFET devices.

VII. SUMMARY

Electronic properties of ZrO₂ and ZrSiO₄ and their interfaces with silicon were investigated using local density functional theory. The calculated electronic band structure, density of states, and band offsets indicate that ZrSiO₄ forms a higher quality interface in terms of electronic properties with adequate conduction and valence band offsets. The ZrO₂/Si interface showed partial occupation of Zr states at the interface and these states may be eliminated by passivating the Zr dangling bonds with hydrogen or having excess oxygen at the interface. All the ZrO₂/Si interfaces showed conduction band offsets of less than or close to 1.00 eV, which could impede the application of ZrO₂ as a gate dielectric layer in MOSFET's. Our calculations suggest that ZrSiO₄ may be an ideal candidate as an alternative gate dielectric, while ZrO₂ will require additional interface preparation to yield adequate electronic properties. It remains to be seen how a ZrSiO₄/Si interface can rearrange in order to reduce lattice-mismatch-induced strain, which we are unable to explore with first principles methods due to the cost of treating a large enough supercell. If, upon rearrangement, these favorable electronic properties remain, then we believe ZrSiO₄ will indeed have a promising future as a gate oxide in microelectronics.

ACKNOWLEDGMENTS

J.P.C. acknowledges financial support from Mattson Technology, the University of California Discovery Grant, the Office of Naval Research, TRW, and UCLA for this work. E.A.C. acknowledges the Air Force Office of Scientific Research for support of this work. The authors are grateful for fruitful discussions with Dr. Ashok Arya and Mr. Vincent Cocula in the Department of Chemistry & Biochemistry at UCLA.

-
- ¹D. A. Buchanan, IBM J. Res. Dev. **43**, 245 (1999).
²G. D. Wilk, R. M. Wallace, and J. M. Anthony, J. App. Phys. **89**, 5243 (2001).
³R. M. C. de Almeida and I. J. R. Baumvol, Surf. Sci. Rep. **49**, 1 (2003).
⁴S.-G. Lim, S. Kriventsov, T. Jackson, J. H. Haeni, D. G. Schlom, A. M. Balbashov, R. Uecker, P. Reiche, J. L. Freeouf, and G. Lucovsky, J. Appl. Phys. **91**, 4500 (2002).
⁵G. D. Wilk, R. Wallace, and G. Anthony, J. Appl. Phys. **87**, 484 (2000).
⁶J. P. Chang and Y.-S. Lin, Appl. Phys. Lett. **79**, 3824 (2001).
⁷J. P. Chang, Y.-S. Lin, S. Berger, A. Kepten, R. Bloom, and S. Levy, J. Vac. Sci. Technol. B **19**, 2137 (2001).
⁸J. P. Chang and Y.-S. Lin, Appl. Phys. Lett. **79**, 3666 (2001).
⁹B.-O. Cho and J. P. Chang, Appl. Phys. Lett. **93**, 745 (2003).
¹⁰K. Parlinski, Z. Li, and Y. Kawazoe, Phys. Rev. Lett. **78**, 4063 (1997).
¹¹G.-M. Rignanese, F. Detraux, X. Gonze, A. Bongiorno, and A. Pasquarello, Phys. Rev. Lett. **89**, 117601 (2002).
¹²Xinyuan Zhao and David Vanderbilt Phys. Rev. B **65**, 075105 (2002).
¹³R. H. French, S. J. Glass, F. S. Ohuchi, Y. N. Xu, and W. Y. Ching, Phys. Rev. B **49**, 5133 (1994).
¹⁴G. Rignanese, F. Detraux, and X. Gonze, Phys. Rev. B **64**, 134301 (2001).
¹⁵G. Rignanese, X. Gonze, and A. Pasquarello, Phys. Rev. B **63**, 104305 (2001).
¹⁶J. Jameson, W. Harrison, and P. Griffin, J. Appl. Phys. **90**, 4570 (2001).
¹⁷B. Kralik, E. K. Chang, and S. G. Louie, Phys. Rev. B **57**, 7027 (1998).
¹⁸A. A. Demkov, Phys. Status Solidi B **226**, 57 (2001).
¹⁹F. Herman and R. Kasowski, J. Vac. Sci. Technol. **19**, 395 (1981).
²⁰M. Hane, Y. Miyamoto, and A. Oshiyama, Phys. Rev. B **41**, 12637 (1990).
²¹T. Yamasaki, C. Kaneta, T. Uchiyama, T. Uda, and K. Terakura,

- Phys. Rev. B **63**, 115314 (2001).
- ²²J. Neaton, D. A. Muller, and N. W. Ashcroft, Phys. Rev. Lett. **85**, 1298 (2000).
- ²³A. Bongiorno, A. Pasquarello, M. S. Hybertsen, and L. C. Feldman, Phys. Rev. Lett. **90**, 186101 (2003).
- ²⁴B. R. Tuttle, Phys. Rev. B **67**, 155324 (2003).
- ²⁵R. B. Laughlin, J. D. Joannopoulos, and D. J. Chadi, Phys. Rev. B **21**, 5733 (1980).
- ²⁶A. X. Chu and W. B. Fowler, Phys. Rev. B **41**, 5061 (1990).
- ²⁷M. M. Banaszak Holl and R. F. McFeely, Phys. Rev. Lett. **71**, 2441 (1993).
- ²⁸M. Lannoo, in *Proceedings of the 173rd Meeting of the Electrochemical Society, Atlanta, 1988*, edited by C. Robert Helms (Plenum Press, New York, 1988), p. 259.
- ²⁹V. Fiorentini and G. Gulleri Phys. Rev. Lett. **89**, 266101 (2002).
- ³⁰F. Giustino, A. Bongiorno, and A. Pasquarello, Appl. Phys. Lett. **81**, 4233 (2002).
- ³¹A. Kawamoto, J. Jameson, P. Griffin, K. Cho, and R. Dutton, IEEE Electron Device Lett. **22**, 14 (2001).
- ³²A. A. Demkov, VLSI Des. **13**, 135 (2001).
- ³³R. A. McKee, Science **293**, 468 (2001).
- ³⁴Cambridge Serial Total Energy Package, distributed by Accelrys Inc., San Diego
- ³⁵V. Milman, B. Winkler, J. A. White, C. J. Pickard, M. C. Payne, E. V. Akhmatkaya, and R. H. Nobes, Int. J. Quantum Chem. **77**, 895 (2000).
- ³⁶P. Hohenberg and W. Kohn, Phys. Rev. **136**, 864 (1964).
- ³⁷W. Kohn and L. Sham, Phys. Rev. **140**, A1133 (1965).
- ³⁸M. C. Payne, M. Teter, D. Allan, T. Arias, and J. Joannopoulos, Rev. Mod. Phys. **64**, 1045 (1992).
- ³⁹Y.-M. Juan and E. Kaxiras, Phys. Rev. B **51**, 9521 (1995).
- ⁴⁰D. Vanderbilt, Phys. Rev. B **41**, 7892 (1990).
- ⁴¹G. Kresse and J. Furthmuller, Phys. Rev. B **54**, 11169 (1996).
- ⁴²C. G. Broyden, Math. Comput. **19**, 577 (1965).
- ⁴³G. D. Wilk and R. Wallace, Appl. Phys. Lett. **76**, 112 (2000).
- ⁴⁴A. Christensen and E. A. Carter, Phys. Rev. B **58**, 8050 (1998).
- ⁴⁵J. D. McCullough and K. N. Truenlood, Acta Crystallogr. **12**, 507 (1959).
- ⁴⁶G. Teufer, Acta Crystallogr. **15**, 1187 (1962).
- ⁴⁷G. P. Srivastava, *Theoretical Modeling of Semiconductor Surfaces* (World Scientific, Singapore, 1999).
- ⁴⁸C. M. Scanlan, M. Gajdardziska-Josifovska, and C. R. Aita, Appl. Phys. Lett. **64**, 3548 (1994).
- ⁴⁹A. Christensen and E. A. Carter, Phys. Rev. B **62**, 16968 (2000).
- ⁵⁰M. D. Segall, R. Shah, C. J. Pickard, and M. C. Payne, Phys. Rev. B **54**, 16317 (1996).
- ⁵¹D. Sánchez-Portal, E. Artacho, and J. M. Soler, Solid State Commun. **95**, 685 (1995).
- ⁵²D. Sánchez-Portal, E. Artacho, and J. M. Soler, J. Phys.: Condens. Matter **8**, 3859 (1996).
- ⁵³R. W. Godby, Top. Appl. Phys. **69**, 51 (1992).
- ⁵⁴R. Puthenkovilakam and J. P. Chang, Appl. Phys. Lett. **84**, 1353 (2004).
- ⁵⁵J. Robertson, J. Vac. Sci. Technol. B **18**, 1785 (2000).
- ⁵⁶H. J. F. Jansen, Phys. Rev. B **43**, 7267 (1991).
- ⁵⁷A. Kawamoto, K. Cho, P. Griffin, and R. Dutton, J. Appl. Phys. **90**, 1333 (2001).
- ⁵⁸V. Milman, D. E. Jesson, and S. J. Pennycook, Phys. Rev. B **50**, 2663 (1994).
- ⁵⁹R. A. Wolkow, Phys. Rev. Lett. **68**, 17 (2636).
- ⁶⁰K. J. Kang and C. B. Musgrave, Phys. Rev. B **64**, 245330 (2001).
- ⁶¹J. Ihm, M. L. Cohen, and D. J. Chadi, Phys. Rev. B **21**, 4592 (1980).
- ⁶²S. Gay, C. A. Jenkins, and G. P. Srivastava, J. Phys.: Condens. Matter **10**, 7751 (1998).
- ⁶³L. S. O. Johansson, R. I. G. Uhrberg, P. Martensson, and G. V. Hansson, Phys. Rev. B **42**, 1305 (1990).
- ⁶⁴R. Wyckoff, *Crystal Structures*, 2nd ed. (Interscience, New York, 1965), Vol. 1, p. 312.
- ⁶⁵H. Kageshima and K. Shiraishi, Surf. Sci. **380**, 61 (1997).
- ⁶⁶H. Kageshima and K. Shiraishi, Surf. Sci. **407**, 133 (1998).
- ⁶⁷C. van de Walle and R. Martin, Phys. Rev. B **35**, 8154 (1987).
- ⁶⁸W. Monch, Phys. Rev. Lett. **58**, 1260 (1987).
- ⁶⁹J. Tersoff, Phys. Rev. Lett. **52**, 465 (1986).
- ⁷⁰N. E. Christensen, Phys. Rev. B **37**, 4528 (1988).
- ⁷¹W. R. L. Lambrecht and B. Segall, Phys. Rev. B **41**, 2832 (1990).
- ⁷²A. Munoz, N. Chetty, and R. M. Martin, Phys. Rev. B **41**, 2976 (1990).
- ⁷³E. V. Stefanovich and A. L. Shluger, Phys. Rev. B **49**, 11 560 (1994).
- ⁷⁴Z. Mursic, T. Vogt, H. Boysen, and F. Frey, J. Appl. Crystallogr. **25**, 519 (1992).
- ⁷⁵R. Ackermann, E. G. Rauh, and C. A. Alexander, High. Temp. Sci. **7**, 304 (1975).